INTERNATIONAL JOURNAL FOR NUMERICAL METHODS IN FLUIDS
Int. J. Numer. Meth. Fluids 2000; **33**: 681–694

Large eddy simulation of fully developed turbulent flow in a rotating pipe

Zhiyin Yang*,[1]

Department of Aeronautical and Automotive Engineering, The University of Loughborough, Loughborough, U.K.

SUMMARY

Large eddy simulation (LES) has been applied to study the fully developed turbulent pipe flow, in particular, to examine the effects of swirl driven by the rotating wall of the pipe. Experimental observations have shown that the intensity of turbulence in the rotating pipe decreases gradually with an increase in rotation rate due to the stabilizing effect of the centrifugal force. These experimentally observed phenomena are confirmed numerically using LES by comparing not only mean velocity profiles but also turbulent intensity and Reynolds stresses at two different rotation rates. The performance of two different subgrid scale models, a dynamical model and the usual Smagorinsky model, has also been assessed for the case of fully developed turbulent swirling flow. A brief description of the numerical methods used with an efficient hybrid Fourier multigrid pressure solver is presented. Particular attention has been paid to the numerical treatment of boundary conditions at the centreline. Copyright © 2000 John Wiley & Sons, Ltd.

KEY WORDS: large eddy simulation; multigrid; rotating pipe flow; swirl

1. INTRODUCTION

Swirling flows are very important phenomena found in nature and they have become of interest in association with a wide range of applications. In non-reactive cases applications include vortex amplifier, cyclone separators, agricultural spraying machines, heat exchangers, etc. In combustion systems, such as in gasoline engines, gas turbines and industrial furnaces, the dramatic effects of swirl to stabilize flames and to improve combustion efficiency have been known and appreciated for many years.

The effects of the swirl driven by the rotating pipe wall on the flow characteristics have been studied experimentally by many researchers and rotation has been found to have a big influence on the suppression of turbulence because of radially growing centrifugal forces.

* Correspondence to: Department of Aeronautical and Automotive Engineering, The University of Loughborough, Loughborough, LE11 3TU, U.K.
[1] E-mail: z.yang@lboro.ac.uk

Received August 1998
Revised August 1999

White [1] and Shchukin [2] observed that the pressure loss decreased with increasing rotational speed. Murakami *et al.* [3], Kikuyama *et al.* [4] and Reich *et al.* [5] measured the mean velocity profiles and wall friction coefficients in the fully developed turbulent flow region for various Reynolds numbers and rotation rates. Their experimental results showed that the mean axial velocity profile gradually approaches a laminar shape with increasing rotation rate. Nishibori *et al.* [6] and Kikuyama *et al.* [7] measured statistics on turbulent fluctuations. However, these statistics were obtained near the entrance of the pipe rather than in the fully developed flow region. Imao and Itoh [8] have recently measured not only mean velocity profiles but also turbulence intensity and Reynolds shear stress in fully developed turbulent flow in an axially rotating pipe. Their detailed measurements provide good validation data for numerical computations and also confirm that when rotation is added to the pipe the turbulence fluctuations are suppressed due to the stabilizing effects caused by the centrifugal force.

It is well established that the conventional two-equation $k-\varepsilon$ model has been successfully applied to many engineering calculations, but it is also well known that its performance becomes poor for certain situations, such as swirling flows [9]. This was verified in an axially rotating pipe flow computation by Hirai *et al.* [10], that the conventional $k-\varepsilon$ model produces very poor results, predicting a solid body rotation profile for the mean circumferential velocity while the experimental studies show that it is not a solid body rotation but similar to a parabolic distribution. It was also shown by Hirai *et al.* [10] that using a $k-\varepsilon$ model modified by the Richardson number to take account of the effects of rotation still produces a solid body rotation profile for the mean circumferential velocity and it is necessary to use full Reynolds stress models for better prediction.

Large eddy simulation (LES) has become a very useful and powerful tool in turbulent flow computations and is being applied to more and more practical engineering problems with the advance of computing power and numerical techniques. However, the literature on LES work in the area of turbulent pipe flow with swirl is very limited. Unger and Friedrich [11] reported, to our knowledge, the first LES of fully developed turbulent pipe flow without swirl. Eggels *et al.* [12] performed direct numerical simulation (DNS) of fully developed turbulent pipe flow without swirl. Orlandi and Fatica [13] have recently reported the DNS of turbulent flow in a rotating pipe and done detailed analysis of their results, relating the drag reduction to the modifications of the near-wall vortical structure. However, the Reynolds number in their study is relatively low and the application of DNS to practical engineering flows is still very limited due to the computing power available now and in the near future. The only LES predictions of fully developed turbulent pipe flow with rotation that we are aware of is that carried out by Eggels and Nieuwstadt [14]. Their numerical results compared reasonably well with the experimental data available at that time, which, however, lacked details of the Reynolds stress field and what was available was not measured in the fully developed flow zone. They also used only a Smagorinsky subgrid scale model in the simulation; how a dynamic subgrid scale model would perform in such a rotating pipe flow case is unknown.

The main objectives of the present paper are firstly, to study numerically the effects of swirl driven by the rotating pipe wall and assess the LES results against the experimental data of Imao and Itoh [8]; and secondly, to compare the performance of two different subgrid scale models, a dynamic model and the Smagorinsky model, in the rotating pipe flow.

2. BASIC EQUATIONS

The first task in LES is to define the large scale components of the flow field, which the method will attempt to calculate directly. There are several ways of doing this mathematically and all are essentially equivalent to averaging the equation over a small region of space or low-pass filtering the equation in Fourier space. Since finite volume method (FVM) with a staggered grid is used in the present study, it makes sense, therefore, to use an approach that arrives at the discretized equations as quickly as possible. The method was originally developed by Deardorff [15] and extended by Schumann [16,17]. The idea is that the equations are integrated over an appropriate control volume and hence the velocity components at the corresponding grid points are interpreted as the volume average. Any small scale (smaller than the mesh or control volume) motions are averaged out and have to be accounted for by a subgrid scale model. For simplicity the incompressible Navier–Stokes equations in Cartesian co-ordinates are presented

$$\frac{\partial \bar{u}_i}{\partial t} = -\frac{1}{\rho}\frac{\partial \bar{p}}{\partial x_i} - \frac{\partial \overline{u_i u_j}}{\partial x_j} + \frac{\partial}{\partial x_j}\nu\left(\frac{\partial \bar{u}_i}{\partial x_j} + \frac{\partial \bar{u}_j}{\partial x_i}\right) \tag{1}$$

The term $\overline{u_i u_j}$ cannot be computed and the difference between it and the part that can be computed, $\bar{u}_i\bar{u}_j$, is the subgrid stress τ_{ij}

$$\tau_{ij} = \overline{u_i u_j} - \bar{u}_i\bar{u}_j \tag{2}$$

which accounts for the unknown small scale (subgrid scale) motions, analogous to the familiar Reynolds stress occurring in the time-averaged Navier–Stokes equations. In contrast to the standard Reynolds stress, whose length and velocity scales are those of the entire turbulent flow field, the length and velocity scales of the subgrid stress are only associated with the small scale motions and can be deduced relatively simply on a local basis from the mesh and the resolved velocity field of the simulation. The earliest estimate for the velocity scale, based on the local strain rate scalar S, proposed by Smagorinsky [18], was $S*\Delta$. He went on to combine these scales into the simple gradient diffusion model that bears his name

$$\tau_{ij} - \delta_{ij}\tau_{kk}/3 = \nu_s\bar{S}_{ij} \tag{3}$$

$$\nu_s = C\Delta^2\bar{S} \tag{4}$$

$$\bar{S} = \sqrt{2\bar{S}_{ij}\bar{S}_{ij}} \tag{5}$$

$$\Delta = \sqrt[3]{\Delta x\Delta y\Delta z} \tag{6}$$

C was predicted theoretically from the Kolmogorov spectrum in homogeneous isotropic turbulence by Lilly [19] to be 0.17^2, which has been proven far too big for wall-bounded shear flows. C is taken to be 0.01 in the present study when the Smagorinsky subgrid scale model is used (with the Van Driest damping near the wall) and it is computed as follows when a dynamic subgrid scale model is employed:

$$C = \frac{\langle L'_{ij} M_{ij} \rangle}{\langle M_{kl} M_{kl} \rangle} \tag{7}$$

$$L_{ij} = T_{ij} - \hat{\tau}_{ij} = \hat{\bar{u}_i \bar{u}_j} - \hat{\bar{u}}_i \hat{\bar{u}}_j \tag{8}$$

$$L'_{ij} = L_{ij} - \delta_{ij} L_{kk}/3 \tag{9}$$

$$M_{ij} = 4\hat{\bar{S}}\hat{\bar{S}}_{ij} - \hat{\bar{S}}\bar{S}_{ij} \tag{10}$$

where the hat indicates that a second filter, usually called the test filter, which is twice the mesh size in the present study, has been applied to the velocity fields. This is a standard procedure and details can be found elsewhere [20,21]; in the present simulation C is averaged in both streamwise and circumferential directions. However, this still cannot guarantee that C will not go negative, although physically one can argue that this means backscatter. Numerically this can cause serious trouble when the total viscosity (sum of subgrid scale eddy viscosity and molecular viscosity) goes negative. In some regions, M_{ij} can be very small or may even approach zero, making Equation (7) poorly conditioned and as a result of this, C can be unrealistically large. In the current simulations, the value of C has been monitored to check that it is not larger than 0.12 or less than 0. It has been found that the computed C in most of the simulation time and most of the computational domain is within this range.

The momentum and continuity equations used in the present study are in a cylindrical co-ordinate system and given below (the overbar is omitted in the following equations for simplicity).

$$\frac{\partial q_x}{\partial t} = -r\frac{\partial p}{\partial x} + \frac{\partial}{\partial x}\left(\tau_{xx} - \frac{q_x q_x}{r}\right) + \frac{\partial}{\partial r}\left(\tau_{xr} - \frac{q_x q_r}{r}\right) + \frac{1}{r}\frac{\partial}{\partial \theta}(\tau_{x\theta} - q_x w) \tag{11}$$

$$\frac{\partial q_r}{\partial t} = -r\frac{\partial p}{\partial r} + \frac{\partial}{\partial x}\left(\tau_{rx} - \frac{q_r q_x}{r}\right) + \frac{\partial}{\partial r}\left(\tau_{rr} - \frac{q_r q_r}{r}\right) + \frac{\partial}{\partial \theta}\left(\tau_{r\theta} - \frac{q_r w}{r}\right) - (\tau_{\theta\theta} - ww) \tag{12}$$

$$\frac{\partial w}{\partial t} = -\frac{1}{r}\frac{\partial p}{\partial \theta} + \frac{1}{r}\frac{\partial}{\partial x}(\tau_{\theta x} - w q_x) + \frac{1}{r^2}\frac{\partial}{\partial r}(r^2 \tau_{\theta r} - r w q_r) + \frac{1}{r}\frac{\partial}{\partial \theta}(\tau_{\theta\theta} - ww) \tag{13}$$

$$\frac{\partial q_x}{\partial x} + \frac{\partial q_r}{\partial r} + \frac{\partial w}{\partial \theta} = 0 \tag{14}$$

where q_x represents axial flux ru (u is the axial velocity), w is the tangential velocity and q_r is radial flux rv (v is the radial velocity), which will be discussed in the next section (why the fluxes are introduced instead of the usual velocity components (u, v)).

The stress are given as follows:

$$\tau_{ij} = 2(\nu + \nu_s) S_{ij} \tag{15}$$

where v_s is the subgrid eddy viscosity given by Equation (4) and S_{ij} in the present study using a cylindrical co-ordinates system are as follows:

$$\begin{bmatrix} S_{xx} & S_{xr} & S_{x\theta} \\ S_{xr} & S_{rr} & S_{r\theta} \\ S_{x\theta} & S_{r\theta} & S_{\theta\theta} \end{bmatrix} = \begin{bmatrix} \dfrac{\partial q_x}{\partial x} & \dfrac{1}{2}\left[\dfrac{\partial q_x}{\partial r}+\dfrac{\partial q_r}{\partial x}-\dfrac{q_x}{r}\right] & \dfrac{1}{2}\left[\dfrac{\partial q_x}{\partial \theta}+r\dfrac{\partial w}{\partial x}\right] \\ S_{xr} & \left[\dfrac{\partial q_r}{\partial r}-\dfrac{q_r}{r}\right] & \dfrac{1}{2}\left[\dfrac{\partial w}{\partial r}+\dfrac{1}{r^2}\cdot\dfrac{\partial q_r}{\partial \theta}-\dfrac{w}{r}\right] \\ S_{x\theta} & S_{r\theta} & \left[\dfrac{1}{r}\cdot\dfrac{\partial w}{\partial \theta}+\dfrac{q_r}{r^2}\right] \end{bmatrix} \tag{16}$$

3. NUMERICAL PROCEDURES

The above governing equations are discretized on a staggered mesh using FVMs. The explicit second-order Adams–Bashforth scheme is used for the momentum advancement except for the pressure term. The second-order central differencing scheme is used for the spatial discretization. The Poisson equation for pressure is solved using an efficient hybrid Fourier multigrid method described in more detail by Voke and Yang [22].

The gains in computational efficiency are generally very significant through the use of Fourier methods. They arise partly because of the reduction of the dimension of the problem and the lack of any connection between the solution for different discrete wavenumbers, and also partly because the higher wavenumber problems have increased diagonal dominance in the solution of Poisson-like equations. This results in greatly accelerated convergence of the higher wavenumber problems and a corresponding saving of computer resource.

Figure 1 shows the computational domain in the present study. The diameter of the pipe is $D = 30$ mm and the length of the computational domain is $4D$. In the circumferential direction, the whole section is simulated. The Reynolds number is 20000 based on the mean axial velocity (denoted as U_m, $\rho * U_m *$area $=$ mass flow rate) and the pipe diameter. All the dimensions and Reynolds number have been chosen to match those of the experiment [8]. The

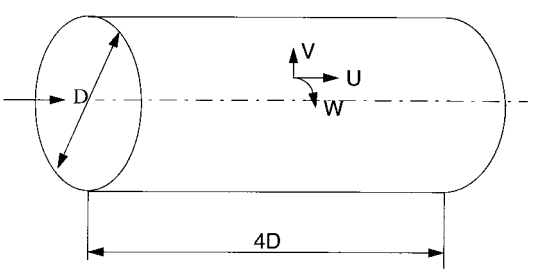

Figure 1. Computational domain.

simulations are carried out with $192*64*128$ grid points (x-, r- and θ-directions respectively) giving $Dx^+ = 30$, Dy^+ varies from 0.75 (nearest to the pipe wall) to 15 and Dz^+ varies from 0.7 (closest to the centre) to 36.

Periodic boundary conditions are applied in the axial direction since the simulated pipe flow is fully developed. The same boundary treatment is applied in the circumferential direction at $\theta = 0°$ and 360°. On the pipe wall the usual no-slip boundary condition is applied. However, owing to the cylindrical co-ordinate system employed in the present study, the governing equations contain a singularity at the centreline of the pipe ($r = 0$), which makes it difficult to specify boundary conditions for all velocity components at the pipe centre. Unger and Friedrich [11] argue that no boundary conditions are needed as the grid surface area goes to zero and therefore the momentum and mass flux is zero too. The present author takes another approach to deal with this by solving the fluxes (r times velocity components) instead of the velocity variables directly as shown in Equations (11)–(14). Therefore, at the centreline, zero is specified for all three variables employed in the equations. Verzicco and Orlandi [23] presented a finite difference scheme in cylindrical co-ordinates, which is similar to the present approach. However, they introduced radial flux only, while both radial and axial fluxes are introduced in the present study. In addition to the singularity at the centreline, the curvature of the cylindrical co-ordinate system can affect the time integration. The time step is restricted by stability criteria to avoid numerical instabilities in all explicit time integration schemes. Since the mesh size in the circumferential direction is proportional to r, it can become quite small towards the centreline. However, due to the present approach employing the fluxes as the variables, the minimum Δz^+ is 0.7, which is not too small and quite close to the minimum Δy^+. It has been found that, in these circumstances, there is no need for all the terms containing derivatives in the circumferential direction to be treated implicitly in time. The dimensionless time step used in the present study is 0.0002 (normalized by D/U_m), which is more or less the same as used for boundary layer transition studies [24,25].

The simulations are initiated from a specified mean axial velocity profile using power-law and random disturbances to mimic the turbulent fluctuations in all three directions. Since the random fluctuations generated in this way are not correlated (white noise with a flat spectrum) they decay more rapidly. Therefore, the initial disturbances need to be stronger than the expected root-mean-square (r.m.s) level but not too strong so as numerical instability may occur. There are alternative ways of avoiding such a rapid decay of artificially generated turbulence, for example, reducing the viscosity initially. The simulations are run sufficiently long to reach a statistically stationary state before the statistics are collected. The final statistics are accumulated by spatial averaging in the homogeneous streamwise and circumferential directions and by time averaging.

Three runs using the Smagorinsky subgrid scale model, one with the pipe wall stationary and another two with the pipe wall rotating at different rates denoted by $N = W_0/U_m$ (0, 0.5, 1.0; W_0 is the tangential velocity of the rotating pipe wall), and two runs using a dynamic subgrid scale model, $N = 0$, 1.0, have been carried out in the present study. Each simulation is usually run for 20000 time steps before the statistics are gathered and run for further 40000 time steps to accumulate the statistics with a sample taken every 20 time steps (2000 samples). One run using the Smagorinsky subgrid scale model takes about 90 CPU hours using one processor on a Cray-YMP machine (one run using the dynamic model takes about 110 CPU hours).

4. RESULTS

The results presented below in Figures 2 and 3 are obtained using the Smagorinsky subgrid scale model.

Figure 2 shows the mean axial velocity profile normalized by the bulk averaged axial velocity U_m versus the radial position normalized by the pipe radius. The simulated results compare reasonably well with the experimental data for all three cases, $N = 0$ (no rotation), $N = 0.5$ and 1.0 (pipe rotating). Both the experimental data and the simulated results show that when the pipe is rotating, axial velocity increases near the centre and decreases near the wall, deforming gradually the fully developed turbulent profile of the axial velocity into a

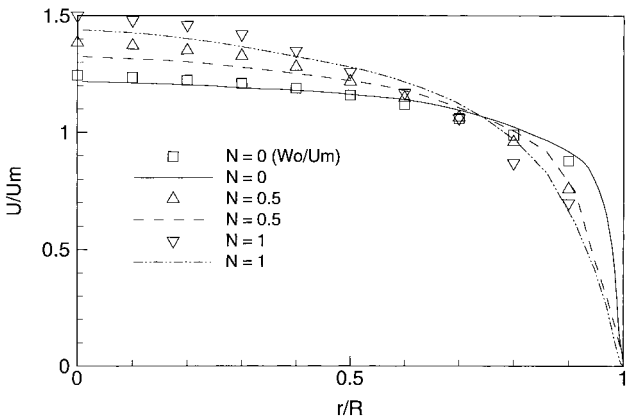

Figure 2. Axial velocity: lines, LES; symbols, experimental data.

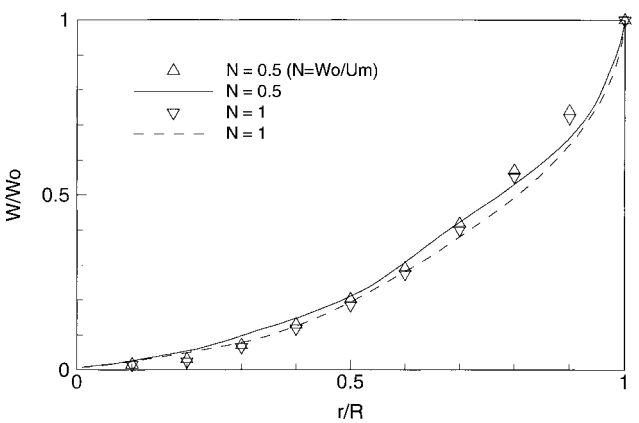

Figure 3. Tangential velocity: lines, LES; symbols, experimental data.

laminar-like profile and decreasing the wall friction force (hence the drag reduction) with an increase in rotation rate, due to the stabilizing effect caused by the centrifugal force. The calculations by Hirai *et al.* [10] employing the conventional $k-\varepsilon$ model failed to predict the tendency of the experimental results, i.e. the predicted mean axial velocity profile at different pipe rotation rates was the same as the profile without rotation.

The comparison between the simulated and the measured tangential velocity profiles normalized by W_0 is shown in Figure 3 for $N = 0.5$, 1.0 and a good agreement has been obtained between the numerical results and the experimental data for both cases. It can be seen form both the LES results and the experimental data that the tangential velocity profile is not a solid body rotation type but is similar to a parabolic distribution, while it is shown by Hirai *et al.* [10] that using the conventional $k-\varepsilon$ model, or even a $k-\varepsilon$ model modified by the Richardson number to account for the effects of rotation would predict a solid body rotation type profile. LES has produced much better results in the present study, as also shown by Orlandi *et al.* [13] and Eggels *et al.* [14] in their LES and DNS studies of rotating pipe flow. It is also worth noting that the profiles under the two rotation rates are more or less the same with little discrepancy between them and it can be said that the profiles are almost independent of rotation rate and Reynolds number as pointed out before by many researchers [4,5,13,14]. However, it is not fully understood yet why the mean circumferential velocity has this universal distribution, independent of Reynolds number and rotation rate.

The results obtained using a dynamic subgrid scale model (for cases $N = 0$ and 1.0) are almost identical and therefore have not been shown. However, there are some differences between predicted turbulence quantities obtained using different subgrid scale models as can be seen in Figures 4–7.

Following the practice by Imao and Itoh [8] in normalizing their experimental data, U_m is also used here as the parameter for normalizing turbulence intensity and Reynolds stress instead of u_τ (friction velocity). The reason for this is that when the pipe is rotating the friction loss reduces due to the stabilizing effect as mentioned above, which means that u_τ decreases. If u_τ is used for normalization Reynolds stress components become large when the pipe is rotating and hence it is difficult to tell the effect of pipe rotation directly. In addition, tangential shear stress exists when the pipe is rotating, which also argues for U_m to be used as the normalization parameter.

Figure 4 shows the axial r.m.s. u'. The experimental data indicate that when the pipe is rotating the streamwise fluctuation decreases a little but not as much as in the LES results. The LES results clearly show that the fluctuation not only reduces when the pipe is rotating but also the peak of the fluctuation shifts slightly away from the wall. This is difficult to confirm from the experimental data as they are not available very near the wall when r/R is larger than 0.9. This tiny shift seems to be present in the LES results by Eggels *et al.* [14] but hardly observable in the DNS results by Orlandi *et al.* [13]. The simulated peak values with both subgrid scale models are quite close to those of the experimental data but the results obtained using the dynamic subgrid scale show a slightly better overall agreement and the peak value especially is closer to the experimental data. However, the numerical results obtained by both subgrid scale models decrease slightly more quickly away from the wall.

The radial and tangential velocity fluctuations are presented in Figures 5 and 6. The numerical results follow the experiment data in that the fluctuations reduce when the pipe is

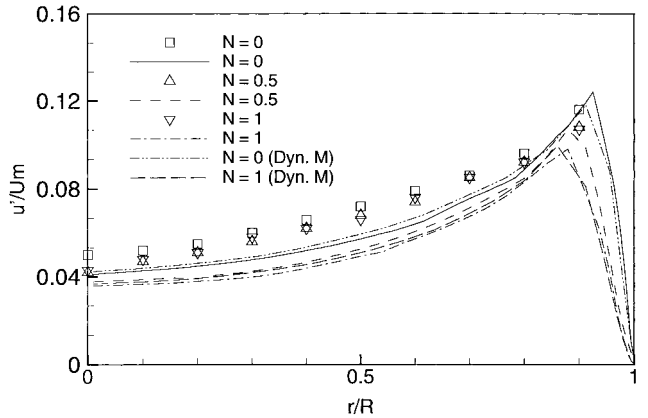

Figure 4. Axial fluctuations: lines, LES; symbols, experimental data.

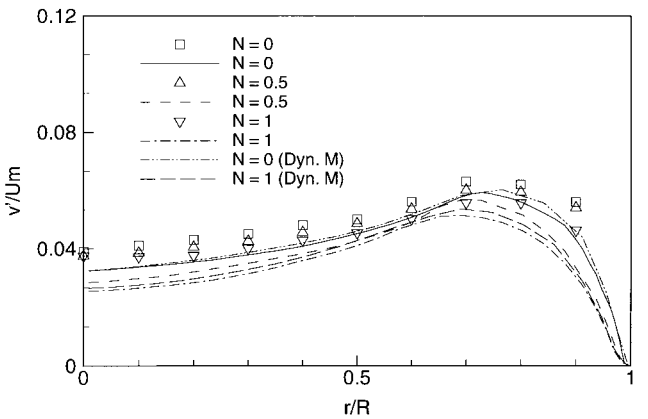

Figure 5. Radial fluctuations: lines, LES; symbols, experimental data.

rotating and a reasonably good agreement has been obtained. It can be seen that the radial component decreases more compared with the other two components. This indicates that the radial fluctuation is the most suppressed, which agrees with the Taylor–Proudman theorem, the turbulent fluctuations perpendicular to the plane of rotation are suppressed because the rotating flow has the tendency of becoming two-dimensional in its plane of rotation. The predicted peak locations for radial and tangential fluctuations, similar to that of the axial component, move away from the wall when the pipe is rotating, which were also clearly shown in the LES results by Eggels *et al.* [14]. Both the LES results and the experimental data clearly show that tangential fluctuations near the wall are actually slightly larger at $N = 1.0$ than those at $N = 0.5$, indicating that it is enhanced rather than suppressed due to rotation. However, the

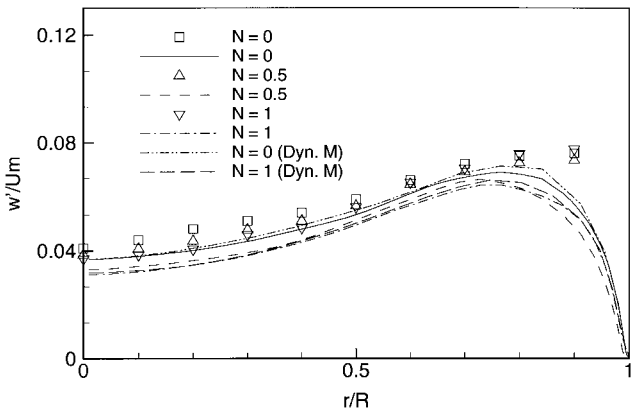

Figure 6. Tangential fluctuations: lines, LES; symbols, experimental data.

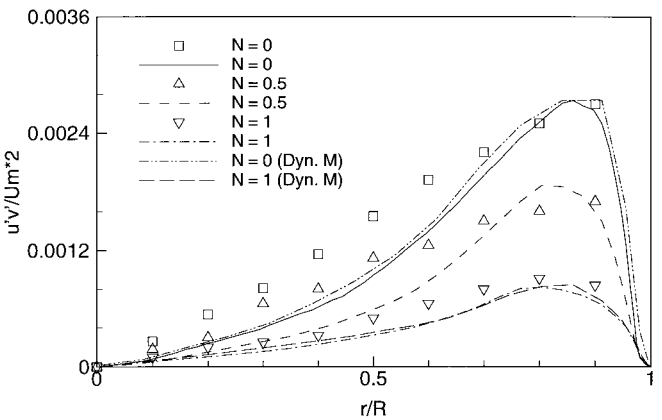

Figure 7. Turbulent shear stress: lines, LES; symbols, experimental data.

simulated results from both subgrid scale models show that the predicted peak values, especially for tangential velocity, are lower than those of the experiment. Again, the results from the dynamic subgrid scale model are slightly better.

The suppressing effect due to the rotation can be more clearly demonstrated by Figure 7, which shows turbulent shear stress. The LES results agree well with the experimental data in the near wall region but reduce more rapidly than the experimental data similar to normal stresses as discussed above. Both the LES results and the experimental data show a considerable reduction when the pipe is rotating. An obvious reduction occurs when the rotation rate changes from 0.5 to 1.0. At $N = 1.0$, its peak value reduces to only about one-third of that without rotation. Again, the simulated results from the dynamic subgrid scale model are slightly better.

One possible explanation for the discrepancy of turbulent fluctuations between the experimental data and the numerical results could be due to lack of mesh resolution away from the wall towards the pipe centre. Another possible reason is that both the subgrid grid scale models are too dissipative, which is true for the Smagorinsky model but not true for the dynamic model. However, the constant obtained from the dynamic model in the present study is averaged over the axial and circumferential directions and has been monitored to check that negative values are not allowed for numerical stability reasons. Therefore, effects of backscatter are not captured in the present study. The averaged subgrid scale eddy viscosity obtained from the dynamic model is slightly smaller (about 10%) than that obtained by the Smagorinsky model, which may explain why the dynamic model gives slightly better results. Better agreement between the numerical results and the experimental data was, indeed, obtained by Eggels *et al*. [12] and Orlandi *et al*. [13] in their DNS studies of turbulent pipe flow. However, their comparison was only limited to the flow without rotation and at relatively low Reynolds numbers.

Figures 8 and 9 show snapshots of the turbulent velocity vectors (v', w') on an (r, θ) plane at $N = 0$ and 1.0. It can be seen from both plots that vortical structures exist in certain regions, which indicates that most of the dynamics occur in those regions. Further away from the wall towards the central region there is much less activity. It is not so obvious to see the effects of pipe rotation from those snapshots but if one examines carefully the region very close to the wall then when the pipe wall is rotating, the near wall region is less turbulent due to the

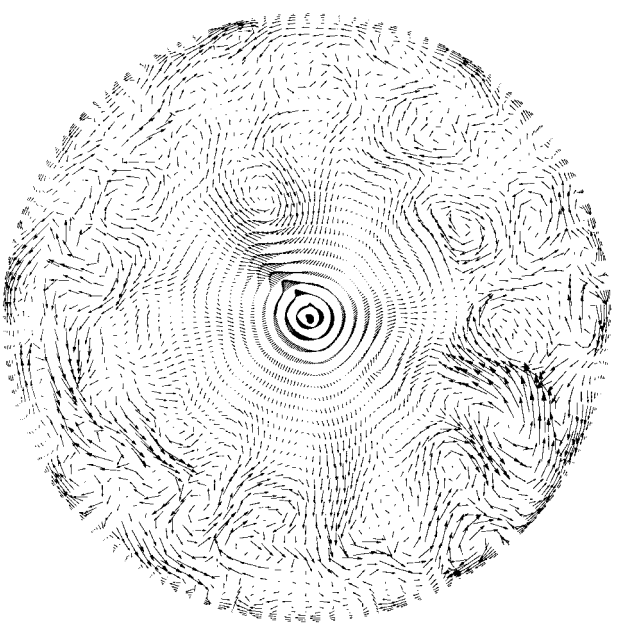

Figure 8. (v', w') vectors at $N = 0$.

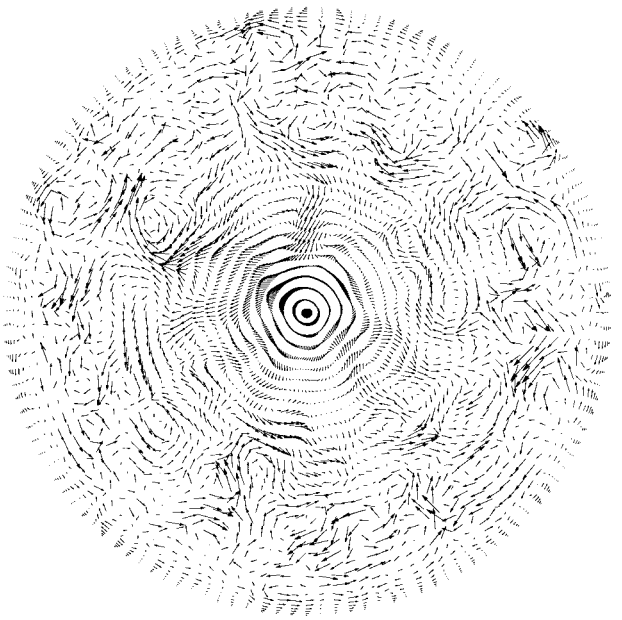

Figure 9. (v', w') vectors at $N = 1$.

suppression of radial fluctuations, and the vortical structures seem to shift a little bit away from the wall, leading to the drag reduction.

5. CONCLUSIONS

Numerical methods for performing LES using a cylindrical co-ordinate system have been described and applied to fully developed turbulent pipe flow with different pipe wall rotation rates. The numerical results compare reasonably well with detailed experimental data and also confirm the experimental observations that turbulence decreases with an increase in pipe rotation due to the stabilizing effect of the centrifugal force. The parabolic distribution of the mean circumferential velocity found in experiments is also reproduced by LES, which any turbulence models using the eddy–viscosity concept would fail to reproduce and would predict a solid body rotation profile as shown by Hirai *et al.* [10].

In the present study, the Smagorinsky subgrid scale model and a dynamic subgrid scale model have been used. However, the performance of the dynamic subgrid scale model is only slightly better than that of the Samogrinsky model in the present study, which may be attributed to the use of a reasonably fine mesh in the near wall region and the turbulent flow being fully developed. It is generally believed that a dynamic model would give better performance for many flow situations such as transitional flow, recirculating flow and flow in

the near wall region. In those situations the flow is under rapid change and a constant C in the Smagorinsky subgrid scale model would not be expected to perform very well and account for the different, complicated flow features.

The mean circumferential velocity has a parabolic profile shape and appears to be proportional to $(r/R)^2$, independent of the Reynolds number and the rotation rates as shown experimentally [3–5,8] and numerically [10,13,14]. However, it is far from fully understood why such a universal velocity distribution exists. Further work is needed to be done to clarify this and more LES data need to be collected to perform detailed analysis confirming that if the relationship between the drag reduction and the change of the near-wall vortical structures at a lower Reynolds number as shown by Orlandi *et al*. [13] in their DNS study of rotating pipe flow exists at higher Reynolds numbers.

ACKNOWLEDGMENTS

The author gratefully acknowledges the useful suggestions and discussions with Professors J.J. McGuirk and P.R. Voke.

REFERENCES

1. White A. Flow of fluid in an axially rotating pipe. *Journal of Mechanical Engineering Science* 1964; **6**: 47–52.
2. Shchukin VK. Hydraulic resistance of rotating tubes. *Journal of Engineering and Physics* 1967; **12**: 418–422.
3. Murakami M, Kikuyama K. Turbulent flow in axially rotating pipes. *Journal of Fluids in Engineering* 1980; **102**: 97–103.
4. Kikuyama K, Murakami M, Nishibori K, Maeda K. Flow in an axially rotating pipe. *Bulletin of the Japan Society of Mechanical Engineers* 1983; **26**(214): 506–513.
5. Reich G, Beer H. Fluid flow and heat transfer in an axially rotating pipe: 1. Effects of rotation on turbulent pipe flow. *International Journal for Heat Mass Transfer* 1989; **32**(3): 551–562.
6. Nishibori K, Kikuyama K, Murakami M. Laminarization of turbulent flow in the inlet region of an axially rotating pipe. *Japan Society of Mechanical Engineers International Journal* 1987; **30**(260): 255–262.
7. Kikuyama K, Murakami M, Nishibori K. Development of three-dimensional turbulent boundary layer in an axially rotating pipe. *Journal of Fluids in Engineering* 1983; **105**: 154–160.
8. Imao S, Itoh M. Turbulent characteristics of the flow in an axially rotating pipe. *International Journal for Heat and Fluid Flow* 1996; **17**: 444–451.
9. Nallasamy M. Turbulence models and their applications to the predictions of internal flows: a review. *Computer and Fluids* 1987; **15**(2): 151–194.
10. Hirai S, Takagi T, Matsumoto M. Prediction of the laminarization phenomena in an axially rotating pipe flow. *Transactions of the ASME, Journal of Fluids in Engineering* 1988; **110**: 424–430.
11. Unger F, Friedrich R. Large eddy simulation of fully-developed turbulent pipe flow. In *Proceedings of Eighth Symposium on Turbulent Shear Flows*, 1991; 19-3-1–19-3-6.
12. Eggels JGM, Unger F, Weiss MH, Westerweel J, Adrian RJ, Friedrich R, Nieuwstadt FTM. Fully developed turbulent pipe flow: a comparison between direct numerical simulation and experiment. *Journal of Fluid Mechanics* 1994; **268**: 175–209.
13. Orlandi P, Fatica M. Direct numerical simulation of turbulent flow in a pipe rotating about its axis. *Journal of Fluid Mechanics* 1997; **343**: 43–72.
14. Eggels EGM, Nieuwstadt FTM. Large-eddy simulation of turbulent flow in an axially rotating pipe. In *Proceedings of the 9th Symposium on Turbulent Shear Flows*, 1993; P310-1–P310-4.
15. Deardorff JW. A numerical study of three-dimensional turbulent channel flow at large Reynolds number. *Journal of Fluid Mechanics* 1970; **41**: 452–480.
16. Schumann U. Results of a numerical simulation of turbulent channel flows. In *International Meeting on Reactor Heat Transfer*, Dalle-Donne M (ed.), 1973; 230–251.
17. Schumann U. Subgrid scale modelling for finite difference simulations of turbulent flows in plane channels and annuli. *Journal of Computers in Physics* 1975; **18**: 376.

18. Smagorinsky J. General circulation experiments with the primitive equations. I. The basic experiment. *Monthly Weather Review* 1963; **91**: 99–164.
19. Lilly DK. On the application of the eddy viscosity concept in the inertial sub-range of turbulence. NCAR Manuscript No. 123, NCAR, Boulder, CO, 1966.
20. Germano M, Piomelli U, Cabot WH. A dynamic subgrid-scale eddy viscosity model. *Physics and Fluids A* 1991; **3**: 1760–1765.
21. Lilly DK. A proposed modification of the Germano subgrid-scale closure method. *Physics and Fluids A* 1992; **4**: 633–635.
22. Voke PR, Yang Z. Hybrid Fourier-multigrid pressure solution method for Navier–Stokes simulations. In *Numerical Methods for Fluid Dynamics V*, Morton KW *et al*. (eds). Oxford University Press: Oxford, 1995; 615–621.
23. Verzicco R, Orlandi P. A finite-difference scheme for three-dimensional incompressible flows in cylindrical coordinates. *Journal of Computers in Physics* 1996; **123**: 402–414.
24. Voke PR, Yang Z. Numerical study of bypass transition. *Physics in Fluids* 1995; **7**: 2256–2264.
25. Yang Z. Large-eddy simulation of separated boundary layer transition. In *Direct and Large-Eddy Simulation II*, Chollet JP, Voke PR (eds). Kluwer: Dordrecht, 1997; 137–146.

